Spin relaxation and Yu-Shiba-Rusinov states in superconducting graphene

Cite as: AIP Conference Proceedings **2551**, 040002 (2022); https://doi.org/10.1063/5.0099040
Published Online: 09 September 2022

Denis Kochan, Michael Barth, Andreas Costa, et al.

Spin Relaxation and Yu-Shiba-Rusinov States in Superconducting Graphene

Denis Kochan,[a] Michael Barth, Andreas Costa, Klaus Richter, and Jaroslav Fabian

Institute for Theoretical Physics, University of Regensburg, 93040 Regensburg, Germany

[a] *Corresponding author: denis.kochan@ur.de*

Abstract We study theoretically the relaxation of quasi-particle spins in graphene in proximity to an *s*-wave superconductor in the presence of resonant magnetic and spin-orbit active impurities. It is well known that off resonance, the relaxation behaves as predicted from superconducting coherence: with lower temperatures the spin relaxation increases when electrons scatter off magnetic impurities (Hebel-Slichter effect), and decreases when the scatterers act via spin-orbit coupling. This distinct temperature dependence, not available in the normal state, can uniquely discriminate between the two scattering mechanisms. We have shown [1] that the Hebel-Slichter picture breaks down when magnetic impurities act resonantly—the emergent Yu-Shiba-Rusinov states inside the gap shift the spectral weight of the magnetic resonances and thus suppress their interaction with quasi-particle states. As a consequence this leads to a significant decrease of the spin-relaxation rate at lower temperatures. Our findings are valid for generic *s*-wave superconductors that host resonant magnetic impurities.

Keywords: superconductivity, graphene, spin relaxation, resonance, Yu-Shiba-Rusinov states, Hebel-Slichter effect

INTRODUCTION

Superconducting spintronics strives at combining both spintronics [2] and superconductivity (SC) [3, 4, 5] to find new phenomena. While the latter can be used as an efficient dissipationless source, the former exploits spin for logical operations. Therefore one can hope to launch a superconducting spin-operating device that would be, on the one hand, very efficient in terms of energy demands, but on the other hand, would offer complex logical performance and fine-tuned functionality. A potentially versatile platform for that is offered by layered, high-mobility 2D materials that are susceptible to superconductivity, while the reduced spatial dimensionality supports topological protection, non-Abelian statistics, and switchable bulk/edge transport. Recent experimental demonstration of SC in twisted bilayer graphene [6], 2D topological insulators [7, 8], and layered transition-metal dichalcogenides [9, 10, 11, 12, 13] drive considerable theoretical and technological interests in that regard.

A limiting factor for spin-based logical performance is spin relaxation (SR) [14, 15, 16, 17, 18, 19, 20, 21, 22, 23]. In this paper we explore *spin relaxation in superconducting graphene (SCG)*, focusing on *magnetic resonant impurities* and *impurities that locally enhance spin-orbit-coupling (SOC)*. Both are, *per se*, at the heart of intense scientific discussions [24, 25, 26, 27, 28, 29, 30] about the dominant SR mechanism in graphene. We demonstrate that *s*-wave SC in graphene could offer an ultimate possibility to discriminate between the possible SR mechanisms. This is because, unlike in the normal phase, the proximity-induced superconducting gap, the strong temperature dependence in carrier population, underlying coherence phenomena, and the potential appearance of bound states all heavily influence the spin-flip dynamics in the superconducting phase. We believe that, despite its experimental challenge, our predictions have the potential to drive forthcoming spintronics activities into the realm of SCG.

Theoretical studies of SCG started more than a decade ago [31, 32]. Soon, it became clear that weak electron-phonon coupling and low electronic densities (at experimentally accessible dopings) are not sufficient to cause the Cooper instability [33, 34, 35]. One possibility to overcome that would be the proximity to a superconductor [36, 37, 38], or alkaline intercalation [39, 40] that enhances the electronic density and also the coupling with phonons. Theoretical models at elevated Fermi energies ($\mu > 1\,\mathrm{eV}$), and especially at regions near the van-Hove singularities ($\mu > 2.7\,\mathrm{eV}$), offer a plethora of 'possible exotic superconducting pairing mechanisms', that count: *p*-wave, extended *s*-wave, (singlet) chiral *d*-wave, (triplet) *f*-wave, and also their simultaneous co-existences; for details see [41, 42, 43, 44, 45, 46, 47, 48]. The first experimental demonstration of SCG [49] dates to 2007, where metallic contacts in a lateral Josephson geometry induced SC in graphene through the proximity effect [50, 51, 52]. However, interfacial geometries in which graphene grows directly on top of a superconductor [53, 54] bring a much higher degree of functionality. At the same time, the predicted superconducting phase in alkaline-intercalated graphite structures was successfully verified [55, 56, 57]. The reported experimental findings vary by method, but the typical magnitudes of

Low-dimensional Materials: Theory, Modeling, Experiment, Dubna 2021
AIP Conf. Proc. 2551, 040002-1–040002-10; https://doi.org/10.1063/5.0099040
Published by AIP Publishing. 978-0-7354-4385-3/$30.00

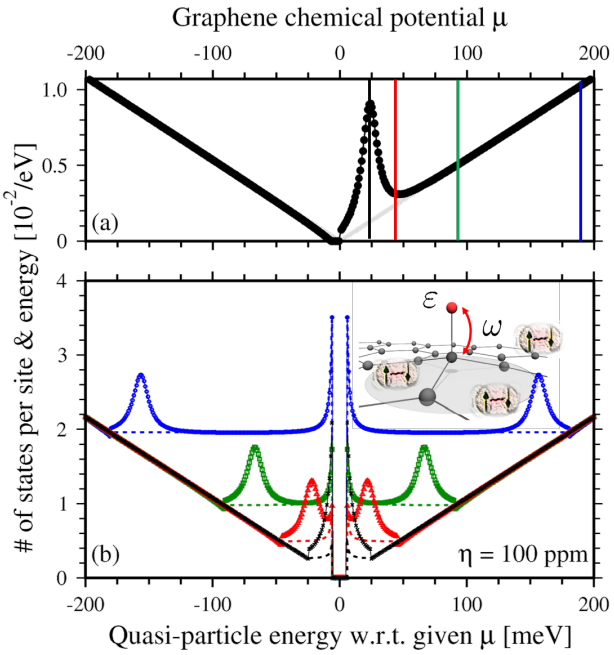

Figure 1. DOS and QP-DOS. Panel (a) displays the DOS in normal graphene (black dots) as a function of the chemical potential (doping level) μ for 100 ppm of resonant impurities. A pronounced resonant peak emerges at $\mu = 24$ meV; the background gray line displays the DOS of the unperturbed system. Black, red, green, and blue vertical lines represent particular resonant and off-resonant chemical potentials, at which we turn the system into its superconducting phase with the superconducting gap $\Delta_0 = 5$ meV. The corresponding QP-DOS at those chemical potentials is shown in (b). Black x-symbols stand for $\mu = 24$ meV, red triangles for $\mu = 45$ meV, green squares for $\mu = 90$ meV, and blue circles for $\mu = 180$ meV. Dashed lines with the same color serve as guides for eyes and display the QP-DOS in the unperturbed SCG. QP resonant enhancement near the coherence peaks appears for chemical potentials close to the resonances in the normal phase. Inset: adatom absorbed on SCG with its pictorial tight-binding description. For all plots we used hybridization $\omega = 5.5$ eV and on-site energy $\varepsilon = 0.26$ eV.

the induced superconducting gap range from few tens of μeV [49] up to 1 meV [58] ($T_c \simeq 7$ K). Also, both *s*-wave [49] and *p*-wave [54] superconducting pairings were convincingly demonstrated; for more details see the comprehensive review [59].

RATIONALE

SR of quasi-particles (QPs) in the superconducting phase depends on the underlying scattering mechanism, namely its time-reversal parity. The latter determines how the electron and hole transition amplitudes combine, before squaring them gives the final spin-flip rate. As pointed out by Yafet [60], the SR rate in the superconducting phase, $1/\tau_s^{\mathrm{SC}}$, relates—within first-order perturbation theory—to its normal phase counterpart, $1/\tau_s^{\mathrm{N}}(E)$, by

$$1/\tau_s^{\mathrm{SC}} \sim \langle (u_{\mathbf{k}} u_{\mathbf{q}} \pm v_{\mathbf{k}} v_{\mathbf{q}})^2 \, 1/\tau_s^{\mathrm{N}} \rangle; \tag{1}$$

for the explicit formula see Eq. (4). Here u and v are the conventional BCS coherence factors, entering the QP wave functions, and $\langle \cdots \rangle$ represents thermal broadening over the QP energies. Consequently, the SR in the superconducting phase can either increase or decrease, depending on the relative sign between the coherence factors. The plus (minus) sign applies to perturbations that are odd (even) w.r.t. time-reversal symmetry, e.g., magnetic impurities (local SOC fields), giving rise to a larger (smaller) $1/\tau_s^{\mathrm{SC}}$ compared to $1/\tau_s^{\mathrm{N}}$. As demonstrated later, those differences for SCG vary with the chemical potential and temperature, and can change by a few orders of magnitude giving an unprecedented experimental feasibility *to disentangle the dominant SR mechanism* by conducting the same experiments in the normal and superconducting phases.

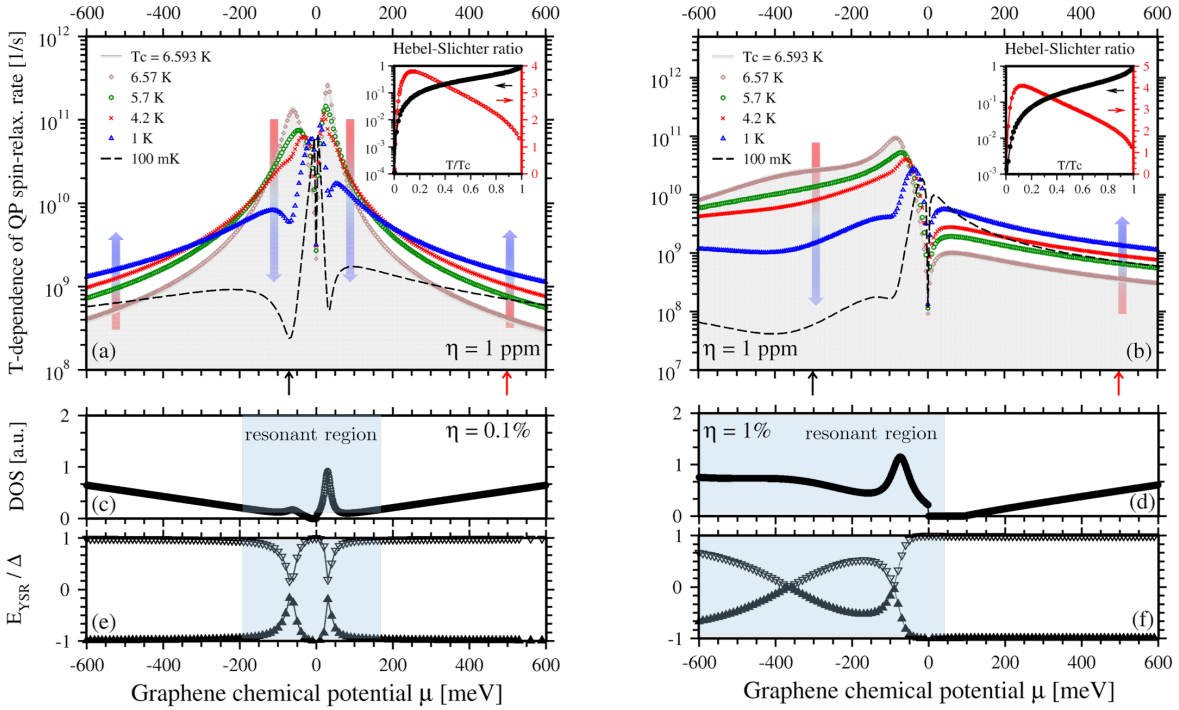

Figure 2. QP-SR rates in SCG at different temperatures (symbols) for 1 ppm of hydrogen (a) and fluorine (b) magnetic impurities as functions of μ. Outside of the resonances the SR rates in the superconducting phase increase in accordance with Yafet's prediction, whereas they decrease in the resonances. Rainbow arrows indicate increasing or decreasing trends of SR rates with lowered T when compared to the normal phase. The insets show the corresponding Hebel-Slichter ratios—$(1/\tau_s^{\mathrm{SC}})/(1/\tau_s^{\mathrm{N}})$ as functions of T/T_{c}—at two representative Fermi energies (indicated by black and red arrow ticks on the horizontal axis): resonant—$\mu = -80$ meV for hydrogen and $\mu = -300$ meV for fluorine—black circled data (values at left logarithmic axis), and off-resonant—$\mu = 500$ meV for both cases—red circled data (values at right linear axis). Panels (c) and (d) show the DOS in the normal phase in the presence of magnetic moments, and resonant (shaded) and off-resonant (white) doping regions; for the sake of visibility the impurity concentrations were exaggerated. Panels (e) and (f) display the energies of the subgap Yu-Shiba-Rusinov states for hydrogen and fluorine as functions of μ. Smaller SR rates in (a) and (b) are correlated with the resonances in the normal phase in (c) and (d), and the bound states in (e) and (f) with energies deep inside the superconducting gap.

The qualitative physical arguments are rather intuitive. QPs have well defined spins, almost unchanged mass from normal-phase carriers, but smaller effective charges, $q = (u^2 - v^2)\,\mathrm{e_{el.}}$, especially in the coherence peaks ($u^2 \simeq v^2$) occupied at $T < T_{\mathrm{c}}$. Consequently, all charge-dominated effects would be less pronounced so that the 'spin-spin exchange' interaction wins over the 'charge-charge direct' interaction and $1/\tau_s^{\mathrm{SC}} > 1/\tau_s^{\mathrm{N}}$. This effect is experimentally known as the Hebel-Slichter effect [61, 62]; for a detailed explanation see [63]. Not only charges of QPs diminish, but also their group velocities, $v_{\mathrm{SC}} \simeq |(u^2 - v^2)|\, v_{\mathrm{N}}$, and hence their momenta. While the SOC couples spins with momenta, the effective strength of the SOC interaction in the superconducting phase significantly decreases, which implies $1/\tau_s^{\mathrm{SC}} < 1/\tau_s^{\mathrm{N}}$. Recent experiments [64, 65] in layered superconducting aluminum reported on significantly lowered SR and attributed that to a weakened SOC in the superconducting phase. For more details about the charge and spin accumulation of QPs in a superconductor, their non-equilibrium separation and relaxation, see Refs. [66, 67, 68]. Despite it is intuitively sound, it is worth to comment on two main limitations of the Yafet relation. First, it does not take into account SR processes that are specific to the superconducting phase, and which lack counterparts above T_{c}, e.g., the formation of YSR states that can take away spectral weight. Second, Yafet's formula a priori breaks at resonances since those are beyond finite-order perturbation theory. Both limitations will be explicitly experienced below.

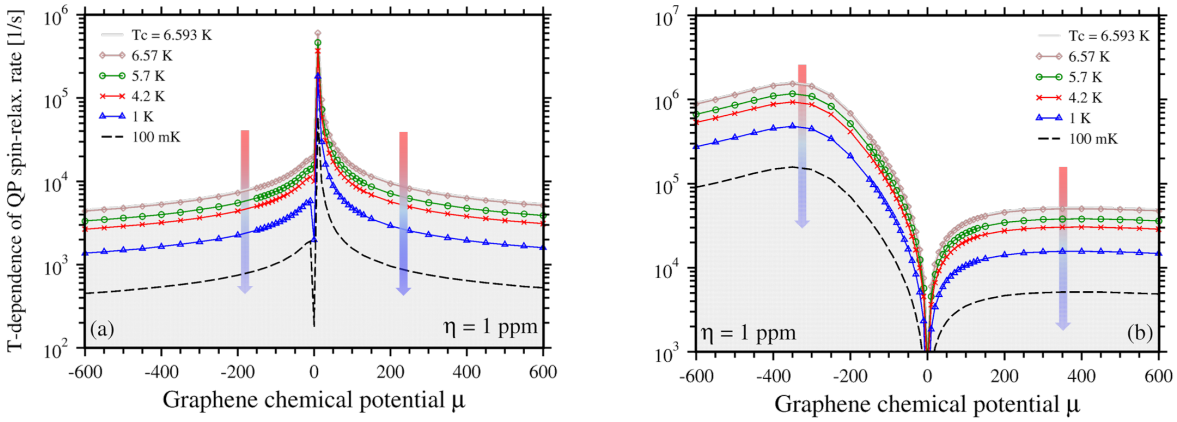

Figure 3. QP-SR rates in SCG at different temperatures (different symbols) due to locally enhanced SOC for 1 ppm of hydrogen (a) and fluorine (b) impurities as functions of μ. With lowering T, the SR rates decrease almost uniformly, their decrease becomes more steep, and would eventually saturate as $T \to 0$. Similarly to the normal phase, the SR rates at resonances are enhanced. Rainbow arrows indicate the decreasing trend of the SR rates with lowered T compared to the normal phase.

MODEL AND METHODOLOGY

To describe the singlet SC in graphene in the proximity to a superconductor we use the established tight-binding model [31]:

$$H_0 = -\sum_{mn\sigma}(t\,\delta_{\langle mn\rangle} + \mu\,\delta_{mn})c^\dagger_{m\sigma}c_{n\sigma} + \Delta\sum_m c^\dagger_{m\uparrow}c^\dagger_{m\downarrow} + \text{h.c.} \tag{2}$$

Here $t = 2.6\,\text{eV}$ stands for the conventional nearest-neighbor hopping, μ for the underlying chemical potential (doping level) with reference at the Dirac point of the normal phase, and Δ for the T-dependent global on-site s-wave-pairing. We assume the BCS temperature dependence of the induced superconducting gap in graphene, $\Delta = \Delta_0 \tanh\left[1.74\sqrt{T_c/T-1}\right]$, with the proximity relevant value of $\Delta_0 = 1\,\text{meV}$ and $T_c \simeq 7\,\text{K}$. Operator $c^{(\dagger)}_{m\sigma}$ annihilates (creates) an electron with spin σ at a graphene lattice site m, δ_{mn} represents the usual Kronecker symbol, and $\delta_{\langle mn\rangle}$ its nearest-neighbor analog—that is unity for direct nearest neighbors and zero otherwise. The orbital interaction with an adatom—annihilation and creation operators d_σ and $d^\dagger_\sigma$—is governed by the hybridization ω, on-site energy ε, and proximity pairing Δ on the impurity site [69]:

$$V_o = \sum_\sigma[(\varepsilon-\mu)d^\dagger_\sigma d_\sigma + \omega d^\dagger_\sigma c_{0\sigma}] + \Delta d^\dagger_\uparrow d^\dagger_\downarrow + \text{h.c.} \tag{3}$$

For a pictorial definition of V_o see the inset in Fig. 1. The above orbital perturbation is completed by a local spin-dependent term V_s. Our analysis covers two experimentally important cases: (1) exchange interaction, $V_s^{(1)} = -J\,\mathbf{S}\cdot\mathbf{s}$, between an itinerant spin $\mathbf{s}$ at the adatom level [70] and a non-itinerant $\frac{1}{2}$ impurity spin $\mathbf{S}$ (e.g., inner shell or Hubbard-like induced), and (2) local SOC in the vicinity of an adatom [71, 72, 73, 74, 75] with enhanced Rashba and pseudospin-inversion asymmetry (PIA) strengths. For the explicit form of $V_s^{(2)}$, see Appendix. To work with realistic impurities we consider hydrogen and fluorine adatoms, as both give sizable SOC enhancement [71, 72] and can also carry magnetic moments [76, 77, 78, 79, 80, 81, 82, 83].

Our methodology is standard: from H_0 at given μ we compute: 1) the eigenspectrum $E_\mathbf{k} = \sqrt{(\varepsilon_\mathbf{k}-\mu)^2+\Delta^2}$, where $\varepsilon_\mathbf{k}$ are the known eigenvalues in the normal phase, 2) 'in' and 'out' scattering states $|\mathbf{k},\sigma\rangle$—QP-Bloch levels normalized to unity, and 3) the unperturbed (retarded) Green's-function elements (normal and anomalous), $\mathbb{G}_0$. From $\mathbb{G}_0$ and $V = V_o + V_s$ we get the T-matrix, $\mathbb{T} = V\cdot(1-\mathbb{G}_0\cdot V)^{-1}$, which gives rise to the scattering amplitudes, $\langle\mathbf{k},\uparrow|\mathbb{T}|\mathbf{q},\downarrow\rangle$, and perturbed Green's function $\mathbb{G} = \mathbb{G}_0 + \mathbb{G}_0\cdot\mathbb{T}\cdot\mathbb{G}_0$. We assume dilute concentration of impurities not affecting the pairing gap Δ [84], what liberates us from self-consistent calculations. Knowing $\mathbb{G}$ we compute the (L)DOS, bound states, and other spectral features of the perturbed system, while from the scattering amplitudes we obtain the spin-flip

scattering rates. Finally, to get SR, $1/\tau_s^{\rm SC}$, at given μ and T for a concentration η (per carbon atom) of spin-active impurities we evaluate the following integral over the 1st Brillouin zone:

$$\frac{1}{\tau_s^{\rm SC}} = \frac{2\eta A_{uc}}{\hbar\pi} \frac{\iint_{\rm BZ} {\rm d}\mathbf{k}\,{\rm d}\mathbf{q}\,|\langle \mathbf{k},\uparrow|\mathbb{T}|\mathbf{q},\downarrow\rangle|^2\,\delta(E_\mathbf{k}-E_\mathbf{q})\left(\frac{\partial g}{\partial E_\mathbf{k}}\right)}{\int_{\rm BZ} {\rm d}\mathbf{k}\left(\frac{\partial g}{\partial E_\mathbf{k}}\right)}, \tag{4}$$

where $g = 1/(\exp[\frac{E_\mathbf{k}}{k_{\rm B}T}]+1)$ is the Fermi-Dirac distribution, and A_{uc} is the area of the graphene unit cell. The Yafet formula, Eq. (1), is as a special case of Eq. (4). Approximating $\mathbb{T} \simeq V$ and plugging the exact expression for the QP-wave functions in terms of the corresponding electronic states in the normal phase (Bogoliubov transformation) one gets $\langle \mathbf{k},\uparrow|V|\mathbf{q},\downarrow\rangle = (u_\mathbf{k}u_\mathbf{q} \pm v_\mathbf{k}v_\mathbf{q})\,(V_s)_{\mathbf{kq}}$, where the last term is the normal-phase matrix element for the spin-flip part of V. Integration over $\mathbf{q}$ gives the SR rate at energy $E_\mathbf{k}$, while integrating over $\mathbf{k}$ accounts for thermal smearing.

RESULTS

Adatoms on graphene give rise to resonances [85, 86, 87, 88]. Particularly those near the Dirac point strongly modify transport properties [88, 89, 90, 91, 92, 93, 94]. Figure 1 demonstrates how resonances in the normal phase affect the population of QP states in SCG. Panel 1(a) shows the density of states (DOS) of graphene covered by 100 ppm of resonant non-magnetic impurities, and panel 1(b) displays the corresponding QP DOS in the superconducting phase for several representative chemical potentials; we use $\omega = 5.5\,$eV, $\varepsilon = 0.26\,$eV, and an enlarged $\Delta_0 = 5\,$meV for better resolution. We present resonant and off-resonant doping limits, and see that whenever μ approaches resonance in the normal phase, the QP-DOS shows strong modification near the coherence peaks in the superconducting phase. This is quite obvious from the BCS point of view; the E-dependence of the QP-DOS at doping level μ relates with the normal DOS at μ via QP DOS$(E) = \frac{E}{\sqrt{E^2-\Delta^2}}\,DOS(\mu)$, so enhanced DOS implies simultaneously enhanced QP-DOS. Since the coherence peaks are important for the transport of QPs and their SR, we expect certain relaxation anomalies at those doping levels that modify them.

Figure 2 shows various characteristics for spin-flip scattering off magnetic impurities in the normal and superconducting graphene for two representative impurities: hydrogen—panels 2(a),(c),(e), and fluorine—panels 2(b),(d),(f). Particularly, Figs. 2(a) and (b) display the QP-SR rates in SCG at $\Delta_0 = 1\,$meV at different temperatures in the presence of 1 ppm of magnetic impurities. We are plotting values of Eq. (4) for $H_0 + V_o + V_s^{(1)}$, varying chemical potential μ, and superconducting gap Δ with temperature T. Hydrogen [70] with magnetic moment—$\omega = 7.5\,$eV, $\varepsilon = 0.16\,$eV and $J = -0.4\,$eV—gives rise to a narrow resonant region near the Dirac point in the normal phase; see the corresponding magnetic DOS in Fig 2(c) [concentration $\eta = 0.1\%$ is exaggerated for the purpose of resolution]. Contrary, fluorine—$\omega = 5.5\,$eV, $\varepsilon = -2.2\,$eV and $J = 0.5\,$eV—develops [72, 82] a wide resonance region spreading down the Dirac point; see the magnetic DOS in Fig 2(d) with concentration $\eta = 1\%$. How those resonances impact the QP-SR rates is seen in Figs. 2(a) and (b). There, the shaded regions show the SR rate in the normal phase ($T = T_{\rm c}$) and that lowering T in the superconducting phase reveals quite an intriguing behavior: for the off-resonant doping regions, $1/\tau_s^{\rm SC} > 1/\tau_s^{\rm N}$ in accordance with the Yafet formula, while at resonances, $1/\tau_s^{\rm SC} \ll 1/\tau_s^{\rm N}$. To quantify those effects we plot in the insets of Figs. 2(a) and (b) the corresponding Hebel-Slichter ratios, $(1/\tau_s^{\rm SC})/(1/\tau_s^{\rm N})$, as functions of $T/T_{\rm c}$. For the representative off-resonant value of $\mu = 500\,$meV, we get in both cases an enhancement of the SR rate in the superconducting phase by almost a factor of 4 (graphs with red symbols), but in the resonant regions—for hydrogen $\mu = -80\,$meV and for fluorine $\mu = -300\,$meV—we see a strong suppression of the SR rates (graphs with black symbols) by almost three-orders of magnitude. This suggests a nice experimental tool—observing enhanced and strongly depleted SR rates in the superconducting phase when varying μ and lowering T would signify the presence of resonant magnetic impurities.

To explain this peculiar decrease of the SR in the resonances, which is at odds with its normal-phase behavior [70, 95], we calculate in Figs. 2(e) and (f) the corresponding energies (T-matrix singularities) of the Yu-Shiba-Rusinov magnetic bound states [96, 97, 98] that emerge in the SCG [99]. We see that these are deep inside the superconducting gap at resonances. This offers an explanation why the SR rates dropped down. The resonant spin-flip scattering of QPs counts many contributions from multiple scatterings and virtual-state tunnelings. Schematically, they can be written as $V_{aa} + V_{aI}\frac{|I\rangle\langle I|}{E_a - E_I + i0_+}V_{Ia} + \cdots$, where E_I represents the energy of any intermediate state—extended or subgap—and E_a stands for the energy of an incident extended QP state. The dominant spin-flip matrix elements,

V_{aI}, are those for which the extended state a overlaps with the magnetic impurity level I=YSR, since only this gives rise to QP-spin flips. While $V_{aI=\mathrm{YSR}}$'s are roughly the same for a-states at the coherence peaks, what matters are the energy differences $E_a - E_{I=\mathrm{YSR}}$ in the denominator. Those are small in the off-resonant region, since $E_{I=\mathrm{YSR}}$ are aligned with the edges of the superconducting gap, and are large in the resonances. That this would cause the reduced SR is also clear from the T-dependence of the SR rates; for higher T the superconducting gap Δ gets smaller and hence also the difference $E_a - E_{I=\mathrm{YSR}}$. It is worth to stress that from the original Yafet formula one would draw the exactly opposite conclusion. This is because the formation of bound states inside the superconducting gap, as well as their role in the virtual scattering processes, were not taken into account. At sub-Kelvin temperatures—data for $T = 100\,\mathrm{mK}$ are displayed by dashed lines in Figs. 2(a) and (b)—the SR rates at low dopings drop down, as QP $\mathrm{DOS}(E) = \frac{E}{\sqrt{E^2-\Delta^2}}\,\mathrm{DOS}(\mu)(-\frac{\partial g}{\partial E})$ becomes substantially suppressed by the thermal Fermi-Dirac smearing. At larger dopings this is countered by higher $\mathrm{DOS}(\mu)$.

Figure 3 shows the SR rates at different temperatures as functions of chemical potential for the Elliott-Yafet [100, 101] SR mechanism—scattering off hydrogen (a) and fluorine (b) impurities in the presence of strong local SOC, $V_s^{(2)}$, which incorporates realistic, first-principles motivated coupling strengths, see Appendix. As predicted by Yafet [60] and quantitatively computed by our full T-matrix calculation, the SR rates for both considered cases decrease with lowered T by an order of magnitude over the whole range of chemical dopings, giving rise to a sizeable signal. Despite that uniform decrease, the SR rates in the resonances get enhanced, as it was also the case in the normal phase [102]. This is because a QP locked in the resonance has enough time to the experience SOC, which can, despite enfeebled in the superconducting phase, flip the QP's spin. As an experimental protocol, a global decrease of the SR rate with lowered T over the whole range of μ would therefore signal SOC-dominated SRs.

CONCLUSIONS

We discussed the SR in graphene in proximity to an s-wave superconductor in the presence of resonant impurities. We demonstrated that, compared to the normal phase, the spin-flip dynamics in the superconducting phase allows to discriminate between the magnetic moment-dominated SR and SOC-dominated one. Our theory predicts that reaching superconducting resonances the former would significantly decrease—alike the *anti-Hebel-Slichter effect*—due to deep-lying subgap Yu-Shiba-Rusinov states. The predicted effect can reach three-to-four orders of magnitude, making it robust and verifiable by experiment.

ACKNOWLEDGMENTS

Authors acknowledge supports from DFG SFB 1277 and the EU Seventh Framework Programme under Grant Agreement No. 604391 Graphene Flagship.

APPENDIX

In the paper we use the local adatom-induced SOC Hamiltonian, $V_s^{(2)}$, that is based on local symmetries [75] and whose couplings are fitted to first-principles calculations; for details concerning hydrogen, see [71], and for fluorine [72]. Since the weak SOC of pristine graphene does not play a significant role we focus on the locally induced

Adatom	$\Lambda_{\mathrm{I}}^{\mathrm{A}}$	$\Lambda_{\mathrm{I}}^{\mathrm{B}}$	Λ_{R}	$\Lambda_{\mathrm{PIA}}^{\mathrm{A}}$	$\Lambda_{\mathrm{PIA}}^{\mathrm{B}}$
Hydrogen	-0.21	0	0.33	0	0.77
Fluorine	0	3.3	11.2	0	7.3

Table I. Spin-orbital tight-binding parameters (in meV) entering the model Hamiltonian $V_s^{(2)}$.

SOC effects in the vicinity of adatoms. The defect region consists of the adatomized carbon ($m = 0$), and sets $\mathrm{C_{nn}}$ and

C_{nnn} of its three nearest (nn) and six next-nearest (nnn) neighbors. A realistic effective SOC Hamiltonian based on local symmetries reads:

$$
\begin{aligned}
V_s^{(2)} = & \frac{i\Lambda_I^A}{3\sqrt{3}} \sum_{m\in C_{nnn}} \sum_{\sigma} c_{0\sigma}^{\dagger} (\hat{s}_z)_{\sigma\sigma} c_{m\sigma} + \text{h.c.} \\
& + \frac{i\Lambda_I^B}{3\sqrt{3}} \sum_{\substack{m,n\in C_{nn} \\ m\neq n}} \sum_{\sigma} c_{m\sigma}^{\dagger} \nu_{mn} (\hat{s}_z)_{\sigma\sigma} c_{n\sigma} \\
& + \frac{2i\Lambda_R}{3} \sum_{m\in C_{nn}} \sum_{\sigma\neq\sigma'} c_{0\sigma}^{\dagger} (\hat{\boldsymbol{s}} \times \boldsymbol{d}_{0m})_{z,\sigma\sigma'} c_{m\sigma'} + \text{h.c.} \\
& + \frac{2i\Lambda_{PIA}^A}{3} \sum_{m\in C_{nnn}} \sum_{\sigma\neq\sigma'} c_{0\sigma}^{\dagger} (\boldsymbol{d}_{0m} \times \hat{\boldsymbol{s}})_{z,\sigma\sigma'} c_{m\sigma'} + \text{h.c.} \\
& + \frac{2i\Lambda_{PIA}^B}{3} \sum_{\substack{m,n\in C_{nn} \\ m\neq n}} \sum_{\sigma\neq\sigma'} c_{m\sigma}^{\dagger} (\boldsymbol{d}_{mn} \times \hat{\boldsymbol{s}})_{z,\sigma\sigma'} c_{n\sigma'} .
\end{aligned}
\tag{5}
$$

Symbol $\hat{s}$ represents an array of the Pauli matrices acting in spin space. The sign factor ν_{mn} equals -1 $(+1)$ if the next-nearest hopping $n \to l \to m$ via a common neighbor l becomes (counter)clockwise and a unit vector $\boldsymbol{d}_{mn} = \frac{\mathbf{R}_m - \mathbf{R}_n}{|\mathbf{R}_m - \mathbf{R}_n|}$ points from site n to m. The first two terms in Eq. (5) are the local intrinsic SOCs associated with sublattices A and B, respectively, the third is the local Rashba SOC, and the last two terms are the local PIA-induced SOC for sublattices A and B, respectively; for more details see [75]. The graphical representation of local SOC hoppings is depicted in Fig. 4. The numerical values of these parameters for hydrogenated and fluorinated graphene are summarized in Table I. We adopted those values in our numerical calculations of SR in the superconducting phase.

REFERENCES

1. D. Kochan, M. Barth, A. Costa, K. Richter, and J. Fabian, "Spin relaxation in *s*-wave superconductors in the presence of resonant spin-flip scatterers," Phys. Rev. Lett. **125**, 087001 (2020).
2. I. Žutić, J. Fabian, and S. Das Sarma, "Spintronics: Fundamentals and applications," Reviews of Modern Physics **76**, 323–410 (2004).
3. M. Eschrig, "Spin-polarized supercurrents for spintronics," Physics Today **64**, 43 (2011).

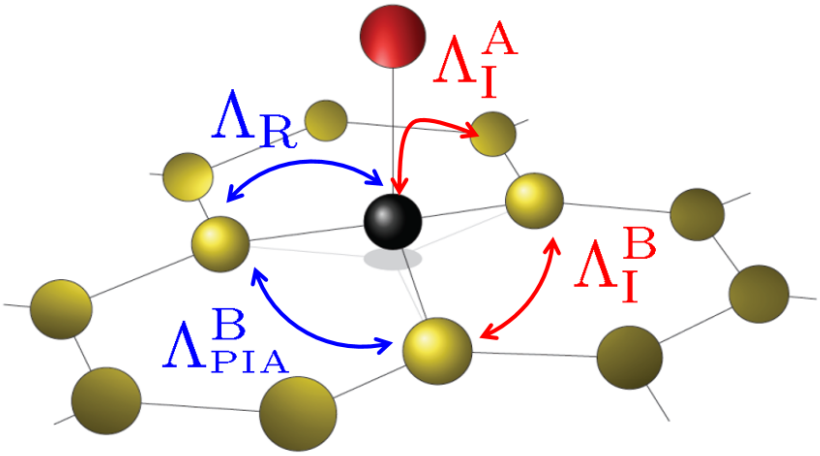

Figure 4. Schematic representation of the local SOC strengths that enter the SOC Hamiltonian $V_s^{(2)}$ in the vicinity of the adatom. Blue and red arrows label spin-flipping and spin-conserving SOC hoppings, respectively, which connect specific nearest or next-nearest neighbor carbons.

4. M. Eschrig, "Spin-polarized supercurrents for spintronics: a review of current progress," Reports on Progress in Physics **78**, 104501 (2015).
5. J. Linder and J. W. A. Robinson, "Superconducting spintronics," Nature Physics **11**, 307–315 (2015).
6. Y. Cao, V. Fatemi, S. Fang, K. Watanabe, T. Taniguchi, E. Kaxiras, and P. Jarillo-Herrero, "Unconventional superconductivity in magic-angle graphene superlattices," Nature **556**, 43–50 (2018).
7. E. Sajadi, T. Palomaki, Z. Fei, W. Zhao, P. Bement, C. Olsen, S. Luescher, X. Xu, J. A. Folk, and D. H. Cobden, "Gate-induced superconductivity in a monolayer topological insulator," Science **925**, 922–925 (2018).
8. V. Fatemi, S. Wu, Y. Cao, L. Bretheau, Q. D. Gibson, K. Watanabe, T. Taniguchi, R. J. Cava, and P. Jarillo-Herrero, "Electrically tunable low-density superconductivity in a monolayer topological insulator," Science **929**, 926–929 (2018).
9. W. Shi, J. Ye, Y. Zhang, R. Suzuki, M. Yoshida, J. Miyazaki, N. Inoue, Y. Saito, and Y. Iwasa, "Superconductivity Series in Transition Metal Dichalcogenides by Ionic Gating," Scientific Reports **5**, 12534 (2015).
10. S. Jo, D. Costanzo, H. Berger, and A. F. Morpurgo, "Electrostatically Induced Superconductivity at the Surface of WS 2," Nano Letters **15**, 1197–1202 (2015).
11. X. Xi, Z. Wang, W. Zhao, J.-H. Park, K. T. Law, H. Berger, L. Forró, J. Shan, and K. F. Mak, "Ising pairing in superconducting NbSe 2 atomic layers," Nature Physics **12**, 139–143 (2016).
12. E. Navarro-Moratalla, J. O. Island, S. Mañas-Valero, E. Pinilla-Cienfuegos, A. Castellanos-Gomez, J. Quereda, G. Rubio-Bollinger, L. Chirolli, J. A. Silva-Guillén, N. Agraït, G. A. Steele, F. Guinea, H. S. J. van der Zant, and E. Coronado, "Enhanced superconductivity in atomically thin TaS2," Nature Communications **7**, 11043 (2016).
13. D. Costanzo, S. Jo, H. Berger, and A. F. Morpurgo, "Gate-induced superconductivity in atomically thin MoS2 crystals," Nature Nanotechnology **11**, 339–344 (2016).
14. N. Tombros, C. Jozsa, M. Popinciuc, H. T. Jonkman, and B. J. van Wees, "Electronic spin transport and spin precession in single graphene layers at room temperature," Nature **448**, 571–574 (2007).
15. M. Ohishi, M. Shiraishi, R. Nouchi, T. Nozaki, T. Shinjo, and Y. Suzuki, "Spin Injection into a Graphene Thin Film at Room Temperature," Japanese Journal of Applied Physics **46**, L605–L607 (2007).
16. K. Pi, W. Han, K. M. McCreary, A. G. Swartz, Y. Li, and R. K. Kawakami, "Manipulation of Spin Transport in Graphene by Surface Chemical Doping," Physical Review Letters **104**, 187201 (2010).
17. T. Y. Yang, J. Balakrishnan, F. Volmer, A. Avsar, M. Jaiswal, J. Samm, S. R. Ali, A. Pachoud, M. Zeng, M. Popinciuc, G. Güntherodt, B. Beschoten, and B. Özyilmaz, "Observation of Long Spin-Relaxation Times in Bilayer Graphene at Room Temperature," Physical Review Letters **107**, 047206 (2011).
18. A. Avsar, T.-Y. Yang, S. Bae, J. Balakrishnan, F. Volmer, M. Jaiswal, Z. Yi, S. R. Ali, G. Güntherodt, B. H. Hong, B. Beschoten, and B. Özyilmaz, "Toward Wafer Scale Fabrication of Graphene Based Spin Valve Devices," Nano Letters **11**, 2363–2368 (2011).
19. M. B. Lundeberg, R. Yang, J. Renard, and J. A. Folk, "Defect-Mediated Spin Relaxation and Dephasing in Graphene," Physical Review Letters **110**, 156601 (2013).
20. M. H. D. Guimarães, P. J. Zomer, J. Ingla-Aynés, J. C. Brant, N. Tombros, and B. J. van Wees, "Controlling Spin Relaxation in Hexagonal BN-Encapsulated Graphene with a Transverse Electric Field," Physical Review Letters **113**, 086602 (2014).
21. B. Raes, J. E. Scheerder, M. V. Costache, F. Bonell, J. F. Sierra, J. Cuppens, J. Van de Vondel, and S. O. Valenzuela, "Determination of the spin-lifetime anisotropy in graphene using oblique spin precession," Nature Communications **7**, 11444 (2016).
22. M. Drögeler, C. Franzen, F. Volmer, T. Pohlmann, L. Banszerus, M. Wolter, K. Watanabe, T. Taniguchi, C. Stampfer, and B. Beschoten, "Spin Lifetimes Exceeding 12 ns in Graphene Nonlocal Spin Valve Devices," Nano Letters **16**, 3533–3539 (2016).
23. S. Dushenko, H. Ago, K. Kawahara, T. Tsuda, S. Kuwabata, T. Takenobu, T. Shinjo, Y. Ando, and M. Shiraishi, "Gate-Tunable Spin-Charge Conversion and the Role of Spin-Orbit Interaction in Graphene," Physical Review Letters **116**, 166102 (2016).
24. P. Seneor, B. Dlubak, M.-B. Martin, A. Anane, H. Jaffres, and A. Fert, "Spintronics with graphene," MRS Bulletin **37**, 1245–1254 (2012).
25. W. Han, R. K. Kawakami, M. Gmitra, and J. Fabian, "Graphene spintronics," Nature Nanotechnology **9**, 794–807 (2014).
26. S. Roche and S. O. Valenzuela, "Graphene spintronics: puzzling controversies and challenges for spin manipulation," Journal of Physics D: Applied Physics **47**, 094011 (2014).
27. S. Roche, J. Åkerman, B. Beschoten, J.-C. Charlier, M. Chshiev, S. Prasad Dash, B. Dlubak, J. Fabian, A. Fert, M. Guimarães, F. Guinea, I. Grigorieva, C. Schönenberger, P. Seneor, C. Stampfer, S. O. Valenzuela, X. Waintal, and B. van Wees, "Graphene spintronics: the European Flagship perspective," 2D Materials **2**, 030202 (2015).
28. Y. P. Feng, L. Shen, M. Yang, A. Wang, M. Zeng, Q. Wu, S. Chintalapati, and C.-R. Chang, "Prospects of spintronics based on 2D materials," Wiley Interdisciplinary Reviews: Computational Molecular Science **7**, e1313 (2017).
29. J. H. Garcia, M. Vila, A. W. Cummings, and S. Roche, "Spin transport in graphene/transition metal dichalcogenide heterostructures," Chemical Society Reviews **47**, 3359–3379 (2018).
30. A. G. Rybkin, A. A. Rybkina, M. M. Otrokov, O. Y. Vilkov, I. I. Klimovskikh, A. E. Petukhov, M. V. Filianina, V. Y. Voroshnin, I. P. Rusinov, A. Ernst, A. Arnau, E. V. Chulkov, and A. M. Shikin, "Magneto-Spin–Orbit Graphene: Interplay between Exchange and Spin–Orbit Couplings," Nano Letters **18**, 1564–1574 (2018).
31. B. Uchoa and A. H. Castro Neto, "Superconducting States of Pure and Doped Graphene," Physical Review Letters **98**, 146801 (2007).
32. N. B. Kopnin and E. B. Sonin, "BCS Superconductivity of Dirac Electrons in Graphene Layers," Physical Review Letters **100**, 246808 (2008).
33. Y. E. Lozovik, S. L. Ogarkov, and A. A. Sokolik, "Theory of superconductivity for Dirac electrons in graphene," Journal of Experimental and Theoretical Physics **110**, 49–57 (2010).
34. Y. Lozovik and A. Sokolik, "Phonon-mediated electron pairing in graphene," Physics Letters A **374**, 2785–2791 (2010).
35. V. N. Kotov, B. Uchoa, V. M. Pereira, F. Guinea, and A. H. Castro Neto, "Electron-Electron Interactions in Graphene: Current Status and Perspectives," Reviews of Modern Physics **84**, 1067–1125 (2012).
36. M. V. Feigel'man, M. A. Skvortsov, and K. S. Tikhonov, "Proximity-induced superconductivity in graphene," JETP Letters **88**, 747–751 (2008).
37. C. W. J. Beenakker, "Colloquium : Andreev reflection and Klein tunneling in graphene," Reviews of Modern Physics **80**, 1337–1354 (2008).
38. P. Burset, A. L. Yeyati, and A. Martín-Rodero, "Microscopic theory of the proximity effect in superconductor-graphene nanostructures," Physical Review B **77**, 205425 (2008).
39. M. Calandra and F. Mauri, "Theoretical Explanation of Superconductivity in C_6Ca," Physical Review Letters **95**, 237002 (2005).

40. G. Profeta, M. Calandra, and F. Mauri, "Phonon-mediated superconductivity in graphene by lithium deposition," Nature Physics **8**, 131–134 (2012).
41. C. Honerkamp, "Density Waves and Cooper Pairing on the Honeycomb Lattice," Physical Review Letters **100**, 146404 (2008).
42. J. González, "Kohn-Luttinger superconductivity in graphene," Physical Review B **78**, 205431 (2008).
43. R. Nandkishore, L. S. Levitov, and A. V. Chubukov, "Chiral superconductivity from repulsive interactions in doped graphene," Nature Physics **8**, 158–163 (2012).
44. M. L. Kiesel, C. Platt, W. Hanke, D. A. Abanin, and R. Thomale, "Competing many-body instabilities and unconventional superconductivity in graphene," Physical Review B **86**, 020507 (2012).
45. R. Nandkishore, R. Thomale, and A. V. Chubukov, "Superconductivity from weak repulsion in hexagonal lattice systems," Physical Review B **89**, 144501 (2014).
46. T. Ma, F. Yang, H. Yao, and H.-Q. Lin, "Possible triplet $p+ip$ superconductivity in graphene at low filling," Physical Review B **90**, 245114 (2014).
47. A. M. Black-Schaffer and C. Honerkamp, "Chiral d -wave superconductivity in doped graphene," Journal of Physics: Condensed Matter **26**, 423201 (2014).
48. J. P. L. Faye, P. Sahebsara, and D. Sénéchal, "Chiral triplet superconductivity on the graphene lattice," Physical Review B **92**, 085121 (2015).
49. H. B. Heersche, P. Jarillo-Herrero, J. B. Oostinga, L. M. K. Vandersypen, and A. F. Morpurgo, "Bipolar supercurrent in graphene," Nature **446**, 56–59 (2007).
50. K. Komatsu, C. Li, S. Autier-Laurent, H. Bouchiat, and S. Guéron, "Superconducting proximity effect in long superconductor/graphene/superconductor junctions: From specular Andreev reflection at zero field to the quantum Hall regime," Physical Review B **86**, 115412 (2012).
51. V. E. Calado, S. Goswami, G. Nanda, M. Diez, A. R. Akhmerov, K. Watanabe, T. Taniguchi, T. M. Klapwijk, and L. M. K. Vandersypen, "Ballistic Josephson junctions in edge-contacted graphene," Nature Nanotechnology **10**, 761–764 (2015).
52. D. I. Indolese, R. Delagrange, P. Makk, J. R. Wallbank, K. Wanatabe, T. Taniguchi, and C. Schönenberger, "Signatures of van Hove Singularities Probed by the Supercurrent in a Graphene-hBN Superlattice," Physical Review Letters **121**, 137701 (2018).
53. C. Tonnoir, A. Kimouche, J. Coraux, L. Magaud, B. Delsol, B. Gilles, and C. Chapelier, "Induced Superconductivity in Graphene Grown on Rhenium," Physical Review Letters **111**, 246805 (2013).
54. A. Di Bernardo, O. Millo, M. Barbone, H. Alpern, Y. Kalcheim, U. Sassi, A. K. Ott, D. De Fazio, D. Yoon, M. Amado, A. C. Ferrari, J. Linder, and J. W. A. Robinson, "p-wave triggered superconductivity in single-layer graphene on an electron-doped oxide superconductor," Nature Communications **8**, 14024 (2017).
55. K. Li, X. Feng, W. Zhang, Y. Ou, L. Chen, K. He, L.-L. Wang, L. Guo, G. Liu, Q.-K. Xue, and X. Ma, "Superconductivity in Ca-intercalated epitaxial graphene on silicon carbide," Applied Physics Letters **103**, 062601 (2013).
56. B. M. Ludbrook, G. Levy, P. Nigge, M. Zonno, M. Schneider, D. J. Dvorak, C. N. Veenstra, S. Zhdanovich, D. Wong, P. Dosanjh, C. Straßer, A. Stöhr, S. Forti, C. R. Ast, U. Starke, and A. Damascelli, "Evidence for superconductivity in Li-decorated monolayer graphene," Proceedings of the National Academy of Sciences **112**, 11795–11799 (2015).
57. J. Chapman, Y. Su, C. A. Howard, D. Kundys, A. N. Grigorenko, F. Guinea, A. K. Geim, I. V. Grigorieva, and R. R. Nair, "Superconductivity in Ca-doped graphene laminates," Scientific Reports **6**, 23254 (2016).
58. P. Rickhaus, M. Weiss, L. Marot, and C. Schönenberger, "Quantum hall effect in graphene with superconducting electrodes," Nano Letters **12**, 1942–1945 (2012).
59. G.-H. Lee and H.-J. Lee, "Proximity coupling in superconductor-graphene heterostructures," Reports on Progress in Physics **81**, 056502 (2018).
60. Y. Yafet, "Conduction electron spin relaxation in the superconducting state," Physics Letters A **98**, 287–290 (1983).
61. L. C. Hebel and C. P. Slichter, "Nuclear Relaxation in Superconducting Aluminum," Physical Review **107**, 901–902 (1957).
62. L. C. Hebel and C. P. Slichter, "Nuclear Spin Relaxation in Normal and Superconducting Aluminum," Physical Review **113**, 1504–1519 (1959).
63. L. C. Hebel, "Theory of Nuclear Spin Relaxation in Superconductors," Physical Review **116**, 79–81 (1959).
64. H. Yang, S.-H. Yang, S. Takahashi, S. Maekawa, and S. S. P. Parkin, "Extremely long quasiparticle spin lifetimes in superconducting aluminium using MgO tunnel spin injectors," Nature Materials **9**, 586–593 (2010).
65. C. H. L. Quay, M. Weideneder, Y. Chiffaudel, C. Strunk, and M. Aprili, "Quasiparticle spin resonance and coherence in superconducting aluminium," Nature Communications **6**, 8660 (2015).
66. H. L. Zhao and S. Hershfield, "Tunneling, relaxation of spin-polarized quasiparticles, and spin-charge separation in superconductors," Physical Review B **52**, 3632–3638 (1995).
67. T. Yamashita, S. Takahashi, H. Imamura, and S. Maekawa, "Spin transport and relaxation in superconductors," Physical Review B **65**, 172509 (2002).
68. C. H. L. Quay, D. Chevallier, C. Bena, and M. Aprili, "Spin imbalance and spin-charge separation in a mesoscopic superconductor," Nature Physics **9**, 84–88 (2013).
69. C. F. Ratto and A. Blandin, "Correlation Effects and Superconductivity in Dilute Alloys with Localized States," Physical Review **156**, 513–521 (1967).
70. D. Kochan, M. Gmitra, and J. Fabian, "Spin Relaxation Mechanism in Graphene: Resonant Scattering by Magnetic Impurities," Physical Review Letters **112**, 116602 (2014).
71. M. Gmitra, D. Kochan, and J. Fabian, "Spin-Orbit Coupling in Hydrogenated Graphene," Physical Review Letters **110**, 246602 (2013).
72. S. Irmer, T. Frank, S. Putz, M. Gmitra, D. Kochan, and J. Fabian, "Spin-orbit coupling in fluorinated graphene," Physical Review B **91**, 115141 (2015).
73. K. Zollner, T. Frank, S. Irmer, M. Gmitra, D. Kochan, and J. Fabian, "Spin-orbit coupling in methyl functionalized graphene," Physical Review B **93**, 045423 (2016).
74. T. Frank, S. Irmer, M. Gmitra, D. Kochan, and J. Fabian, "Copper adatoms on graphene: Theory of orbital and spin-orbital effects," Physical Review B **95**, 035402 (2017).
75. D. Kochan, S. Irmer, and J. Fabian, "Model spin-orbit coupling Hamiltonians for graphene systems," Physical Review B **95**, 165415 (2017).

76. O. V. Yazyev, "Emergence of magnetism in graphene materials and nanostructures," Reports on Progress in Physics **73**, 056501 (2010).
77. L. Xie, X. Wang, J. Lu, Z. Ni, Z. Luo, H. Mao, R. Wang, Y. Wang, H. Huang, D. Qi, R. Liu, T. Yu, Z. Shen, T. Wu, H. Peng, B. Özyilmaz, K. Loh, A. T. S. Wee, Ariando, and W. Chen, "Room temperature ferromagnetism in partially hydrogenated epitaxial graphene," Applied Physics Letters **98**, 193113 (2011).
78. X. Hong, K. Zou, B. Wang, S.-H. Cheng, and J. Zhu, "Evidence for Spin-Flip Scattering and Local Moments in Dilute Fluorinated Graphene," Physical Review Letters **108**, 226602 (2012).
79. R. R. Nair, M. Sepioni, I.-L. Tsai, O. Lehtinen, J. Keinonen, A. V. Krasheninnikov, T. Thomson, A. K. Geim, and I. V. Grigorieva, "Spin-half paramagnetism in graphene induced by point defects," Nature Physics **8**, 199–202 (2012).
80. H. Gonzalez-Herrero, J. M. Gomez-Rodriguez, P. Mallet, M. Moaied, J. J. Palacios, C. Salgado, M. M. Ugeda, J.-Y. Veuillen, F. Yndurain, and I. Brihuega, "Atomic-scale control of graphene magnetism by using hydrogen atoms," Science **352**, 437–441 (2016).
81. K. Szałowski, "Critical temperature of two-dimensional hydrogenated multilayer graphene-based diluted ferromagnet," Carbon **108**, 327–334 (2016).
82. S. Wellnhofer, A. Stabile, D. Kochan, M. Gmitra, Y.-W. Chuang, J. Zhu, and J. Fabian, "Spin relaxation in fluorinated single and bilayer graphene," Phys. Rev. B **100**, 035421 (2019).
83. F. J. Sousa, B. Amorim, and E. V. Castro, "Dilute magnetism in graphene," arXiv:1901.08614.
84. M. J. Zuckermann, "Resonance Scattering in Impure Superconductors," Physical Review **140**, A899–A905 (1965).
85. Y. V. Skrypnyk and V. M. Loktev, "Local spectrum rearrangement in impure graphene," Physical Review B **75**, 245401 (2007).
86. T. O. Wehling, S. Yuan, A. I. Lichtenstein, A. K. Geim, and M. I. Katsnelson, "Resonant Scattering by Realistic Impurities in Graphene," Physical Review Letters **105**, 056802 (2010).
87. A. Ferreira and E. R. Mucciolo, "Critical Delocalization of Chiral Zero Energy Modes in Graphene," Physical Review Letters **115**, 106601 (2015).
88. S. Irmer, D. Kochan, J. Lee, and J. Fabian, "Resonant scattering due to adatoms in graphene: Top, bridge, and hollow positions," Physical Review B **97**, 075417 (2018).
89. Y. V. Skrypnyk and V. M. Loktev, "Electrical conductivity in graphene with point defects," Physical Review B **82**, 085436 (2010).
90. A. Ferreira, T. G. Rappoport, M. A. Cazalilla, and A. H. Castro Neto, "Extrinsic Spin Hall Effect Induced by Resonant Skew Scattering in Graphene," Physical Review Letters **112**, 066601 (2014).
91. A. A. Stabile, A. Ferreira, J. Li, N. M. R. Peres, and J. Zhu, "Electrically tunable resonant scattering in fluorinated bilayer graphene," Physical Review B **92**, 121411 (2015).
92. J. H. Garcia and T. G. Rappoport, "Kubo–Bastin approach for the spin Hall conductivity of decorated graphene," 2D Materials **3**, 024007 (2016).
93. J. Katoch, T. Zhu, D. Kochan, S. Singh, J. Fabian, and R. K. Kawakami, "Transport Spectroscopy of Sublattice-Resolved Resonant Scattering in Hydrogen-Doped Bilayer Graphene," Physical Review Letters **121**, 136801 (2018).
94. J. Lee, D. Kochan, and J. Fabian, "Interplay of resonant states and Landau levels in functionalized graphene," Physical Review B **99**, 035412 (2019).
95. D. Kochan, S. Irmer, M. Gmitra, and J. Fabian, "Resonant Scattering by Magnetic Impurities as a Model for Spin Relaxation in Bilayer Graphene," Physical Review Letters **115**, 196601 (2015).
96. L. Yu, "Bound State in Superconductors with Paramagnetic Impurities," Acta Physica Sinica **21**, 75–91 (1965).
97. H. Shiba, "Classical Spins in Superconductors," Progress of Theoretical Physics **40**, 435–451 (1968).
98. A. I. Rusinov, "Superconcductivity near a Paramagnetic Impurity," JETP Letters **9**, 85 (1969).
99. J. L. Lado and J. Fernández-Rossier, "Unconventional Yu–Shiba–Rusinov states in hydrogenated graphene," 2D Materials **3**, 025001 (2016).
100. R. J. Elliott, "Theory of the Effect of Spin-Orbit Coupling on Magnetic Resonance in Some Semiconductors," Physical Review **96**, 266–279 (1954).
101. Y. Yafet, *Solid state Physics - Advances in Research and Applications*, edited by F. Seitz and D. Turnbull, Vol. 14 (Academic Press, New York, London, 1963) pp. 2–96.
102. J. Bundesmann, D. Kochan, F. Tkatschenko, J. Fabian, and K. Richter, "Theory of spin-orbit-induced spin relaxation in functionalized graphene," Physical Review B **92**, 081403 (2015).